Detection of VHE Bridge emission from the Crab pulsar with the MAGIC Telescopes

T. Saito
Kyoto University, Kyoto, 606-8052 Japan
S. Bonnefoy
Universidad Complutense, Madrid, E-28040 Spain
K. Hirotani
Academia Sinica, Institute of Astronomy and Astrophysics (ASIAA), Taipei, P.O. Box: 23-141 Taiwan
R. Zanin on behalf of the MAGIC Collaboration
Universitat de Barcelona, ICC, IEEC-UB, Barcelona, E-08028 Spain

The Crab pulsar is the only astronomical pulsed source detected above 100 GeV. The emission mechanism of very high energy gamma-ray pulsation is not yet fully understood, although several theoretical models have been proposed. In order to test the new models, we measured the light curve and the spectra of the Crab pulsar with high precision by means of deep observations. We analyzed 135 hours of selected MAGIC data taken between 2009 and 2013 in stereoscopic mode. In order to discuss the spectral shape in connection with lower energies, 4.6 years of Fermi-LAT data were also analyzed. The known two pulses per period were detected with a significance of 8.0 σ and 12.6 σ. In addition, significant bridge emission was found between the two pulses with 6.2 σ. This emission can not be explained with the existing theories. These data can be used for testing new theoretical models.

1. Introduction

The Crab pulsar and the surrounding Crab nebula are the remnant of the supernova of AD 1054. Both the pulsar and the nebula are well studied in a very wide energy range starting from radio (10^{-5} eV) to VHE energies (up to tens of TeV). It is one of the youngest pulsars known and its spin down luminosity (4.6×10^{38} erg/s) is the highest among Galactic neutron stars. To date, this pulsar is the only one for which pulsed emission has been detected above 100 GeV.

Gamma-ray pulsation from the Crab pulsar up to $\sim$ 10 GeV had been known since the 1990s [Nolan et al. 1993]. In 2008, pulsations were detected by the MAGIC telescope at energies above 25 GeV [Aliu et al. 2008]. This result suggested that the emission originates in the outer magnetosphere. The simplest curvature radiation scenario in the outer magnetosphere predicts an exponential cutoff in the energy spectrum at GeV energies [e.g., Muslimov and Harding 2004, Takata et al. 2006, Tang et al. 2008]. Fermi-LAT observations from 100 MeV to a few tens of GeV, which started in August 2008, showed a clear break in the spectrum at $\sim$ 6 GeV [Abdo et al. 2010] supporting this scenario. A few years later, however, MAGIC and VERITAS [Aleksić et al. 2011, 2012a, Aliu et al. 2011] found that the energy spectrum of the Crab pulsar extends up to 400 GeV following a power law. The emission above 100 GeV is difficult to explain only with the curvature radiation, and additional or different emission mechanisms are required. Several new models were recently proposed to explain the energy spectrum of the Crab pulsar [e.g., Aleksić et al. 2011, Aharonian et al.

2012].

Here we present new results from the continuing monitoring of the Crab pulsar with the MAGIC telescopes that will help to constrain any model for the emission. In order to discuss the Crab pulsar spectra at energies lower than those accessible to MAGIC, Fermi-LAT data were also analyzed.

2. Instruments, data sets, and analysis methods

2.1. The MAGIC Telescopes

The MAGIC telescopes are two Imaging Atmospheric Cherenkov Telescopes located on the island of La Palma (Spain) at 2200 m above sea level. Both telescopes consist of a 17 m diameter reflector and a fast imaging camera with a field of view of 3.5°. The trigger threshold for regular observations at zenith angles below 35° is around 50 GeV and the sensitivity above 290 GeV (in 50 h) is 0.8% of the Crab nebula flux with an angular resolution better than 0.07° [Aleksić et al. 2012b].

For this study we used 135 hours of data taken at zenith angles below 35° during optimal technical and weather conditions between September 2009 and April 2013. Standard MAGIC analysis, as described in Moralejo et al. [2009] and Aleksić et al. [2012b], was applied to the data. The conversion from event arrival times to pulsar rotational phases used Tempo2 software [Hobbs et al. 2006] and a dedicated package inside MARS [López 2006]. The spin parameters of the Crab pulsar were taken from the monthly reports of

the Jodrell Bank Radio telescope[1] [Lyne et al. 1993].

2.2. *Fermi*-LAT

The Large Area Telescope (LAT) is a pair conversion gamma-ray detector on board the *Fermi* satellite [Atwood et al. 2009]. It can detect high-energy gamma rays from 20 MeV to more than 300 GeV. It has been operational since August 2008 and all the collected data are publicly available. In this work, we have used 5.5 years of Pass 7 reprocessed data[2] from 2008 August 4 to 2014 January 31. The region of interest was chosen to be $30°$ around the Crab pulsar.

Along with the public data, the LAT team provides the corresponding analysis software and instrument response functions (IRF) designed for the analysis of that particular dataset. We have used the version v9r32p5 of the *Fermi*-LAT ScienceTools[3] and the P7REP_SOURCE_V15 IRF. From the downloaded data we have discarded events taken at zenith angles above $100°$ to reduce the contamination of albedo gamma rays coming from the Earth's limb. To compute the pulse phase, we used the same spin parameters as for the MAGIC analysis. The obtained fluxes were computed by maximizing the likelihood of a given source model using the gtlike tools. The binned likelihood method was adopted and a $40°$ square area with $0.2°$ bin width was used for the likelihood maximization. Apart from the Galactic (gal_iem_v05.fits) and extragalactic (iso_source_v05.txt) diffuse emission, we considered as background sources for the likelihood fits all sources listed in the second LAT source catalogue [Nolan et al. 2012]. The data taken during the periods when the Crab nebula was flaring were not excluded from the analysis. These flares should not have any impact on the pulsed emission results because it is known that the pulsation component did not change during the flares [Buehler et al. 2012], and the average nebula flux including flare periods was subtracted when the pulsar signal was determined. Regarding the reported Fermi-LAT spectrum from the Crab nebula, the six Crab flares that lasted a few days might be responsible for a few percent of the photons below 1 GeV in the overall 5.5 year dataset. Given that the effect is expected to be small, and that this paper focusses on the emission from the pulsar, we did not correct for this effect.

---

3. Results

3.1. Light curve above 50 GeV

Figure 1 shows the light curves of the Crab pulsar measured by MAGIC. Two peaks are clearly visible. Following our previous study [Aleksić et al. 2012a], we define phase ranges for the two peaks as $P1_M$ (phase -0.017 to 0.026) and $P2_M$ (0.377 to 0.422). The background level (hadrons and continuum gamma rays) is estimated using the phase range between 0.52 and 0.87 and it is then subtracted from the histograms[4]. The number of excess events in $P1_M$ between 50 GeV and 400 GeV is 930 ± 120 ($8.0\,\sigma$) and in $P2_M$ is 1510 ± 120 ($12.6\,\sigma$).

In addition to the two main peaks, significant emission between them is also visible. The region between the peaks is generally called the Bridge. Defining the Bridge region as the gap between $P1_M$ and $P2_M$, namely, between 0.026 and 0.377 (hereafter $Bridge_M$), we obtain an excess of 2720 ± 440 ($6.2\,\sigma$) events in this region. Adopting the definition used at lower energies for the Bridge as the region $0.14 - 0.25$ from Fierro et al. [1998] (hereafter $Bridge_E$), then the number of excess events is 880 ± 200 ($4.4\,\sigma$). This excess increases to 1940 ± 370 ($5.2\,\sigma$) if we extend $Bridge_E$ with the so-called trailing wing of P1 and the leading wing of P2, namely to the interval of $0.04 - 0.32$ [see Fierro et al. 1998]. It should be noted that this detection confirms the hint of bridge emission already reported in [Aleksić et al. 2012a].

3.2. Comparison with lower energies

Figure 2 shows the light curves at optical, X-ray, and gamma-ray energies obtained with various instruments, together with the $50-400$ GeV light curve from the bottom panel of Fig. 1. The background was subtracted in the same way as the MAGIC light curves (see Sect. 3.1). The intensity and morphology of the bridge emission varies considerably with energy. It is very weak at optical wavelengths and in the $100-300$ MeV range, while there is an appreciable difference at X-rays and soft gamma rays. At the energies covered by MAGIC, the peaks become much sharper and a prominent bridge emission appears.

It is known that the flux ratio between the two peaks strongly depends on energy, as does the ratio between the first peak and the bridge [see, e.g., Kuiper et al. 2001]. Fig. 3 shows the flux ratio between $P2_M$ and $P1_M$ and that between $Bridge_E$ and $P1_M$ as a function of energy from optical (~ 2 eV)

---

[4] An estimation of the background using the off-peak interval from the LAT Second Pulsar Catalog, namely the phase range between 0.61 and 0.89, lead to very similar results.
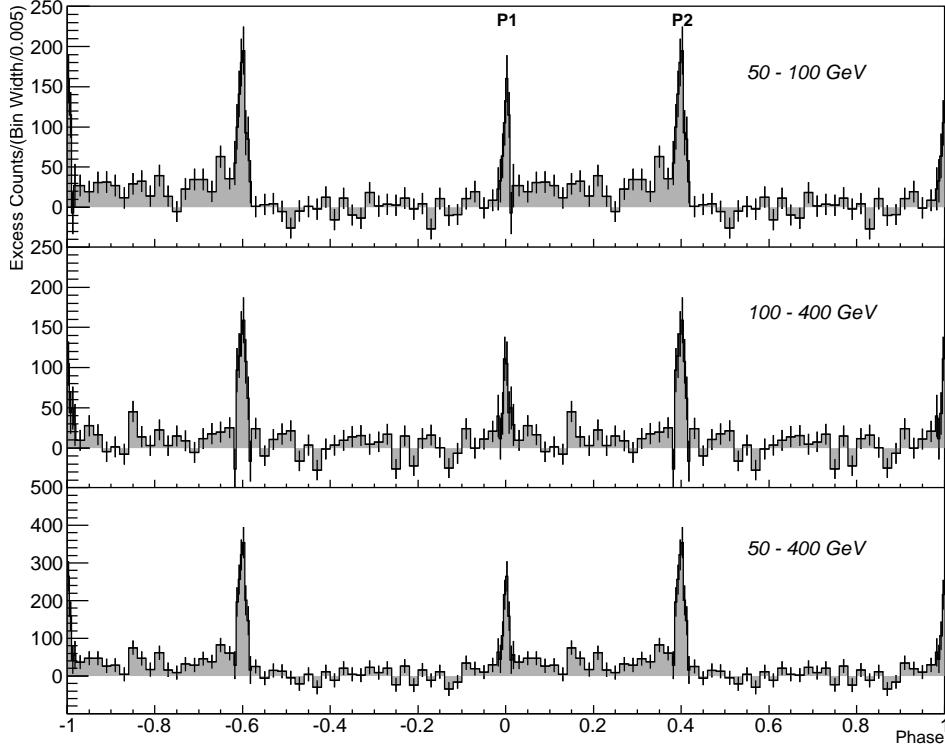
Figure 1: Light curves of the Crab pulsar obtained by MAGIC from 50 GeV to 100 GeV (top), from 100 GeV to 400 GeV (middle), and for the full analyzed energy range (bottom). The bin widths around the peaks are 4 times smaller (0.005) than the rest (0.02) in order to highlight the sharpness of the peaks.

to 400 GeV. Steady emission was subtracted before the ratios were computed. The ratios $P2_M/P1_M$ and $Bridge_E/P1_M$ behave similarly. These ratios increase with energy up to 1 MeV, decrease up to 100 MeV, and increase again from that energy on. At $50 - 400$ GeV, the ratios basically follow the trend seen at lower energies.

3.3. Spectral energy distribution

The spectral energy distributions (SEDs) of the $P1_M$, $P2_M$, $Bridge_M$, and $Bridge_E$ between 100 MeV and 400 GeV are shown in Fig. 4, together with the Crab nebula SED obtained with a subset of the data used for the pulsar analysis. The SEDs were calculated using *Fermi*-LAT data below 50 GeV (below 200 GeV for the nebula), and MAGIC data above 50 GeV. The nebula SED is connected smoothly between the two instruments. The *Fermi*-LAT data were fit with a power law with an exponential cutoff, while the MAGIC data were fit with a simple power-law function. The obtained fit parameters are summarized in Table I. The power-law indices between 50 GeV and 400 GeV are about 3 and no significant difference is seen between different pulse phases. The uncertainty in the absolute energy scale is estimated as 17%,

whereas the systematic error of the flux normalization is estimated to be 18%. We estimate the overall systematic uncertainty uncertainty on the spectral slope to be 0.3.

4. Discussion

In summary, the Crab pulsar above 50 GeV exhibits a light curve with a significant bridge emission between two sharp peaks (Fig. 1). The flux ratios $P2_M/P1_M$ and $Bridge_E/P1_M$ increase with increasing photon energy between 100 MeV and 400 GeV (Figs. 2 and 3). Between 30 GeV and 400 GeV, the fluence in the bridge phase is comparable to that in the P1 phase (Fig. 4). The SEDs in the $50 - 400$ GeV range could be fit with power-law functions for the three phases.

There are several models which can explain the VHE emission of the Crab pulsar, such as Aleksić et al. [2011], Aharonian et al. [2012], Bednarek [2012], Arka and Dubus [2013], Chkheidze et al. [2013]. However, none of them can explain the VHE pulse profile and the spetrum consistently. Further theoreticaly studies and deeper observations of the Crab and other gamma-ray pulsars are needed to understand the VHE emission

Table I Spectral Parameters

phase	$F_1{}^a$ $_{[10^{-11}\mathrm{MeV}^{-1}\mathrm{cm}^{-2}\mathrm{s}^{-1}]}$	$\Gamma_1{}^a$	$E_c{}^a$ $_{[\mathrm{GeV}]}$	$F_{100}{}^b$ $_{[10^{-11}\mathrm{TeV}^{-1}\mathrm{cm}^{-2}\mathrm{s}^{-1}]}$	$\Gamma_2{}^b$
$\mathrm{P1_M}$	8.87 ± 0.14	1.88 ± 0.01	3.74 ± 0.15	4.18 ± 0.59	3.25 ± 0.39
$\mathrm{P2_M}$	3.14 ± 0.07	1.97 ± 0.01	7.24 ± 0.64	8.48 ± 0.62	3.27 ± 0.23
$\mathrm{Bridge_M}$	7.70 ± 0.11	1.74 ± 0.01	7.19 ± 0.39	12.2 ± 3.3	3.35 ± 0.79
$\mathrm{Bridge_E}$	0.95 ± 0.04	1.44 ± 0.04	6.94 ± 0.90	3.7 ± 1.1	3.51 ± 0.97

[a]Parameters obtained by fitting a function $F(E) = F_1(E/1\mathrm{GeV})^{-\Gamma_1}\exp(E/E_c)$ to *Fermi*-LAT data between 100 MeV and 300 GeV

[b]Parameters obtained by fitting a function $F(E) = F_{100}(E/100\mathrm{GeV})^{-\Gamma_2}$ to MAGIC data between 50 GeV and 400 GeV
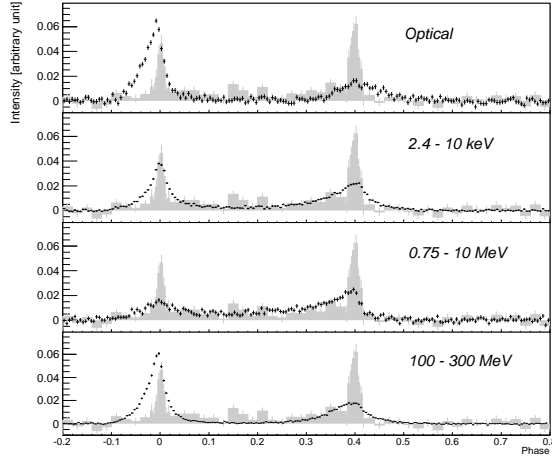

Figure 2: Light curve of the Crab pulsar at optical wavelength, $2.4 - 10$ keV X-rays, $0.75 - 10$ MeV, and $100 - 300$ MeV gamma rays (from top to bottom). The light curve at $50 - 400$ GeV is overlaid on each plot for comparison. The optical light curve was obtained with the MAGIC telescope using the central pixel of the camera [Lucarelli et al. 2008]. The keV and MeV light curves are from Kuiper et al. [2001]. The $100 - 300$ MeV light curve was produced using the *Fermi*-LAT data. All light curves are zero-suppressed by estimating the background using the events in the phase range from 0.52 to 0.87.

mechanism of pulsars.

Acknowledgments
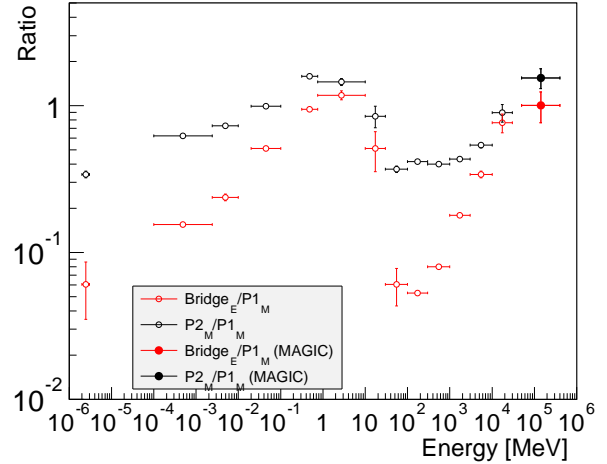
Figure 3: $\mathrm{P2_M}/\mathrm{P1_M}$ ratio (black markers) and $\mathrm{Bridge_E}/\mathrm{P1_M}$ ratio (red markers) as a function of energy. At optical energies (a few eV), the ratios are obtained using the central pixel of the MAGIC camera [Lucarelli et al. 2008]. From 100 eV to 100 MeV, ratios are computed based on the light curves shown in Kuiper et al. [2001]. From 100 MeV to 30 GeV, *Fermi*-LAT data were used.
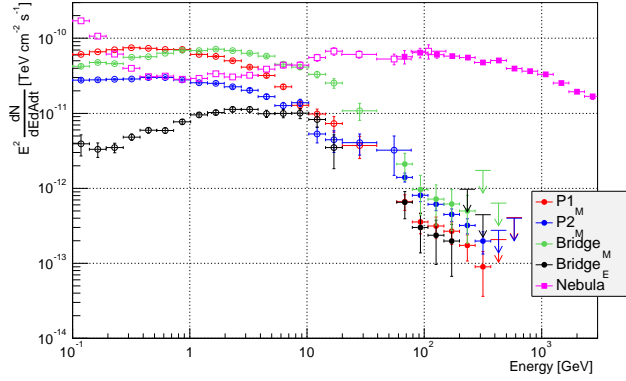
Figure 4: Spectral energy distributions of the Crab nebula, P1$_M$, P2$_M$, Bridge$_M$, and Bridge$_E$ measured with *Fermi*-LAT (below 50 GeV) and MAGIC (above 50 GeV). The flux values averaged over the rotation period are plotted.

References

P. L. Nolan, Z. Arzoumanian, D. L. Bertsch, J. Chiang, C. E. Fichtel, J. M. Fierro, R. C. Hartman, S. D. Hunter, G. Kanbach, D. A. Kniffen, et al., ApJ **409**, 697 (1993).

E. Aliu, H. Anderhub, L. A. Antonelli, P. Antoranz, M. Backes, C. Baixeras, J. A. Barrio, H. Bartko, D. Bastieri, J. K. Becker, et al., Science **322**, 1221 (2008), 0809.2998.

A. G. Muslimov and A. K. Harding, ApJ **606**, 1143 (2004), astro-ph/0402462.

J. Takata, S. Shibata, K. Hirotani, and H.-K. Chang, MNRAS **366**, 1310 (2006), astro-ph/0511690.

A. P. S. Tang, J. Takata, J. J. Jia, and K. S. Cheng, ApJ **676**, 562 (2008), 0711.2719.

A. A. Abdo, M. Ackermann, M. Ajello, W. B. Atwood, M. Axelsson, L. Baldini, J. Ballet, G. Barbiellini, M. G. Baring, D. Bastieri, et al., ApJ **708**, 1254 (2010), 0911.2412.

J. Aleksić, E. A. Alvarez, L. A. Antonelli, P. Antoranz, M. Asensio, M. Backes, J. A. Barrio, D. Bastieri, J. Becerra González, W. Bednarek, et al., ApJ **742**, 43 (2011), 1108.5391.

J. Aleksić, E. A. Alvarez, L. A. Antonelli, P. Antoranz, M. Asensio, M. Backes, J. A. Barrio, D. Bastieri, J. Becerra González, W. Bednarek, et al., A&A **540**, A69 (2012a), 1109.6124.

E. Aliu, T. Arlen, T. Aune, M. Beilicke, W. Benbow, A. Bouvier, S. M. Bradbury, J. H. Buckley, V. Bugaev, K. Byrum, et al., Science **334**, 69 (2011), 1108.3797.

F. A. Aharonian, S. V. Bogovalov, and D. Khangulyan, Nature **482**, 507 (2012).

J. Aleksić, E. A. Alvarez, L. A. Antonelli, P. Antoranz, M. Asensio, M. Backes, J. A. Barrio, D. Bastieri, J. Becerra González, W. Bednarek, et al., Astroparticle Physics **35**, 435 (2012b), 1108.1477.

A. Moralejo, M. Gaug, E. Carmona, P. Colin, C. Delgado, S. Lombardi, D. Mazin, V. Scalzotto, J. Sitarek, D. Tescaro, et al., ArXiv e-prints (2009), 0907.0943.

G. B. Hobbs, R. T. Edwards, and R. N. Manchester, MNRAS **369**, 655 (2006), arXiv:astro-ph/0603381.

M. López, Ph.D. thesis, Universidad Complutense de Madrid, https://magicold.mpp.mpg.de/publications/theses/MLopezMoya.pdf (2006).

A. G. Lyne, R. S. Pritchard, and F. Graham-Smith, MNRAS **265**, 1003 (1993).

W. B. Atwood, A. A. Abdo, M. Ackermann, W. Althouse, B. Anderson, M. Axelsson, L. Baldini, J. Ballet, D. L. Band, G. Barbiellini, et al., ApJ **697**, 1071 (2009), 0902.1089.

P. L. Nolan, A. A. Abdo, M. Ackermann, M. Ajello, A. Allafort, E. Antolini, W. B. Atwood, M. Axelsson, L. Baldini, J. Ballet, et al., ApJS **199**, 31 (2012), 1108.1435.

R. Buehler, J. D. Scargle, R. D. Blandford, L. Baldini, M. G. Baring, A. Belfiore, E. Charles, J. Chiang, F. D'Ammando, C. D. Dermer, et al., ApJ **749**, 26 (2012), 1112.1979.

J. M. Fierro, P. F. Michelson, P. L. Nolan, and D. J. Thompson, ApJ **494**, 734 (1998), arXiv:astro-ph/9709123.

F. Lucarelli, J. A. Barrio, P. Antoranz, M. Asensio, M. Camara, J. L. Contreras, M. V. Fonseca, M. Lopez, J. M. Miranda, I. Oya, et al., Nuclear Instruments and Methods in Physics Research A **589**, 415 (2008).

L. Kuiper, W. Hermsen, G. Cusumano, R. Diehl, V. Schönfelder, A. Strong, K. Bennett, and M. L. McConnell, A&A **378**, 918 (2001), arXiv:astro-ph/0109200.

W. Bednarek, MNRAS **424**, 2079 (2012), 1205.4855.

I. Arka and G. Dubus, A&A **550**, A101 (2013), 1208.2819.

N. Chkheidze, G. Machabeli, and Z. Osmanov, ApJ **773**, 143 (2013).